KfK 5408
November 1994

Strength and Fatigue Measurements for CfC Materials

T. Fett, H. Schneider
Institut für Materialforschung
Projekt Kernfusion

Kernforschungszentrum Karlsruhe

KERNFORSCHUNGSZENTRUM KARLSRUHE
Institut für Materialforschung
Projekt Kernfusion

KfK 5408

Strength and Fatigue Measurements for CfC Materials

T. Fett, H. Schneider

Kernforschungszentrum Karlsruhe GmbH, Karlsruhe

Kernforschungszentrum Karlsruhe GmbH
Postfach 3640, 76021 Karlsruhe

ISSN 0303-4003

Strength and fatigue measurements for CfC materials

Abstract

CfC-materials are considered as candidate materials for the divertors of fusion reactors as well as for protecting tiles of the first wall. As a consequence of cyclic thermal loading the mechanical failure modes will be spontaneous failure due to exceeding of the limit of strength and failure caused by cyclic fatigue. These two failure modes are of main interest to the experimental investigations on CfC-materials. The mechanical behaviour of several CfC-materials was studied applying different types of testing: strength measurements, determination of fatigue and recording of crack-resistance curves.

Messung der Festigkeit und der Ermüdung an CfC

Kurzfassung

CfC-Materialien werden für den Divertor und den Schutz der ersten Wand von Fusionsreaktoren in Erwägung gezogen. Durch den periodischen Betrieb des Reaktors und die dadurch hervorgerufenen periodischen thermischen Spannungen kann es zum Versagen der CfC-Bauteile kommen. Dabei ist sowohl mit sofortigem Versagen durch Erreichen der Kurzzeitfestigkeit wie auch mit verzögertem Versagen infolge von Materialermüdung zu rechnen. Aus diesem Grunde wurden das Festigkeits- und Ermüdungsverhalten untersucht.

Contents

1. Introduction 1

2. Materials 2

3. Development of test devices 3

3.1 Specimen fixing for bending tests at room temperature 3

3.2 High-temperature, high-vacuum testing device 4
3.2.1 Testing machine 4
3.2.2 Heater and vacuum device 5
3.2.3 Four-point-bending fixture 5

3.3 Fatigue test arrangement 7

3.4 Low-compliance bending test for R-curve determination 8

4. Results 11

4.1 Bending strength at room temperature 11

4.2 High-temperature bending strength 17

4.3 Cyclic fatigue 17
4.3.1 Cyclic fatigue of graphite 17
4.3.2 Cyclic tests with SEP-N112 18

4.4 R-curves 18

5. Microstructure 21

5.1 Microstructural investigation by optical microscopy 21

5.2 Microstructural investigation with the scanning electron microscope 21

6. References **26**

7. Appendix **27**

7.1 Elastic moduli 27

1. Introduction

CfC-materials are considered as candidate materials for the divertors of fusion reactors as well as for protecting tiles of the first wall. During operation of the reactor, the divertor is periodically heated at the operating frequency leading to $\simeq 1 \cdot 10^4$ cycles. In order to reduce the maximum heat peak, the thermal load is "swept" at a frequency of $\simeq$ 1Hz resulting in $\simeq 1 \cdot 10^7$ cycles. The surface temperatures are expected to occur in the range of $T_{max} = 1000°C$ to 1200°C. The temperature gradient from the surface to the cooling tube gives rise to thermal stresses, which may cause failure. As the consequence of thermal loading the mechanical failure modes will be

- spontaneous failure due to exceeding the limit of strength,
- failure caused by cyclic fatigue.

It was the aim of KfK-activities (PKF/3A4R) conducted within the "European Fusion Technology Programme" (Subtask PPM 1.3) to develop test devices and to performe tests to characterise several CfC-materials. Since KfK will finish the activities related to CfC at the end of 1994, this report may be understood as the final report on this topic.
The appropriate tests to characterise the material resistance are:

1. Bending strength measurements for the description of spontaneous failure,
2. determination of crack-resistance curves (R-curves), because this effect generally improves the strength behaviour of brittle materials,
3. fatigue experiments in bending.

These two failure modes are of main interest in the experimental investigations and it was planned to carry out the related experiments for three CfC-materials SEPCARB N 112, provided by NET, one material F3333, provided by KfK, and a series of carbon specimens delivered by KfA Jülich.
In order to allow the experiments to be performed, several testing devices had to be developed. These were:

1. Test facilities for cyclic fatigue at room temperature,
2. a high-temperature and vacuum testing device for strength and for cyclic fatigue measurements,
3. a test arrangement with extremely low compliance for crack resistance measurements.

In principle, a material would be characterised sufficiently if all tests such as strength, fatigue and crack-resistance tests would be carried out for all three directions of a CfC-block between room temperature and 1500°C. Due to the limited number of specimens which could be prepared from the delivered blocks (maximum block size 104x50x30mm³), not all tests could be performed with all materials.

2. Materials

The following materials were taken into consideration:

- CfC: FMI 3333, manufacturer FMI Composites Ltd (Galashiels, Scotland). A series of 3.5x4.5x45mm bending bars were provided by KfK (Prof. Dienst, IMF I).
- CfC: SEPCARB N112, Manufacturer, SEP (Bordeaux, France). A cylinder of this material was provided by NET (J. van der Laan). This material will be called N112A below.
- CfC: SEPCARB N112, Manufacturer, SEP (Bordeaux, France). One block (104x50x30 mm^3) was provided by NET (J. van der Laan). It will be denoted as N112B
- CfC: SEPCARB N112, Manufacturer, SEP (Bordeaux, France). Two blocks were delivered by NET (Prof. Wu) and are denoted as N112C.
- Graphite: 25 bending bars of fine graphite EK98 were provided by KfA Jülich, IRW (Prof. Koizlik).

Also at other KfK institutes strength data of CfC-materials were determined:

- CfC: SEPCARB N112, Manufacturer, SEP (Bordeaux, France). Measurements carried out at IMF I (Prof. Dienst, Dr. H. Zimmermann) will be reported here. The material was provided by KfK and will be termed N112D. The measurements of its elastic modulus will be given in the Appendix.

3. Development of test devices

3.1 Specimen fixing for bending tests at room temperature

The bending strength of brittle materials is normally measured in 4-point-bending. For CfC-materials some problems appear in bending tests. In 4-point and 3-point bending tests the specimens may be damaged directly below the inner rollers due to the high local stresses occurring at these points ([1]-[3]). As a consequence of the variable bending moment outside the inner roller span shear stresses must occur which may cause delamination effects. Such effects can be avoided by application of cantilever loading similar to that used in the cyclic fatigue tests. In order to minimise notch effects and localised loads, the bending specimens (1) were fixed in brass tubes (2) with an epoxy resin (3) (UHU plus endfest 300) as illustrated in Fig.1b.

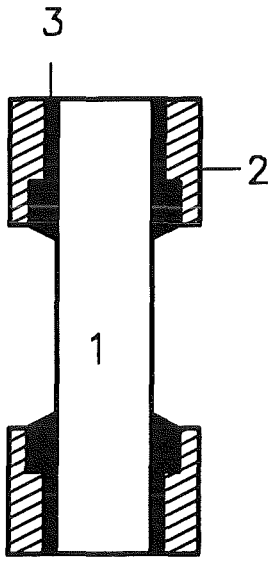

Figure 1. . Specimen for a bending strength test.

The preparation of the specimens shown in fig.1 is schematically described in fig.2. At one front side the bending bar is glued onto a flat metal plate with an adhesive prepared on the basis of cyanogen acrylate (a). A short cylindrical shell made of brass

(8mm diameter, ≃1mm thickness) is also fixed concentrically to the longitudinal axis of the specimen with an adhesive that allows to adjust the tube to be adjusted to its correct position within about 1 minute (b). We used a two-component epoxy resin (UHU-sofortfest). After some minutes, the gap between the brass tube and the specimen can be filled with a 2-component epoxy resin of higher strength (UHU endfest 300) (c). The epoxy may be hardened at higher temperature (≃90°C) in order to reduce the duration of curing. Then the specimen has to be disconnected from the metal plate, for instance with universal pliers applied at the brass tube. The procedure is then repeated at the other end of the bending bar where the sequence of the specimen and tube fixing on the metal plate has to be changed.

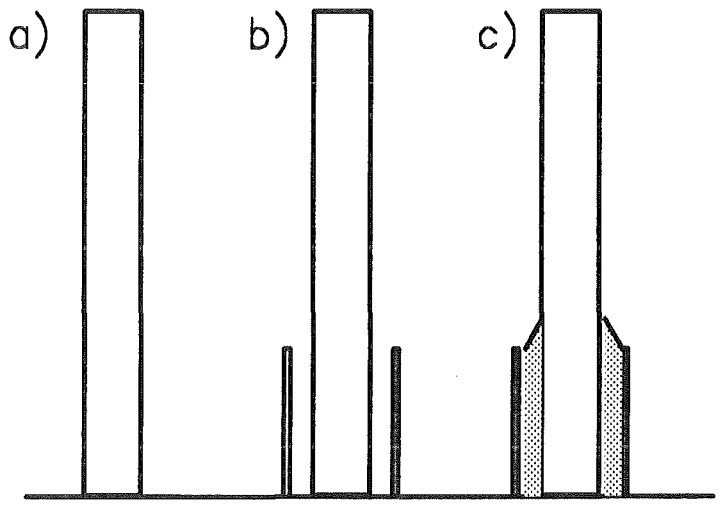

Figure 2. . Preparation of the bending specimens.

3.2 High-temperature, high-vacuum testing device

3.2.1 Testing machine

The high-temperature, high-vacuum device is used to investigate the strength of CfC at high temperatures and in a controlled environment.
The facility (see fig.3) consists of a servohydraulic testing machine (Type INSTRON 1251) with a 5000N load cell and a maximum frequency for cyclic fatigue experiments of 50Hz. Machine control for load rate, strain rate or position experiments can be performed by a digital control unit. A personal computer is used to read out data which are logged by the control unit. The maximum data logging frequency is 5000 points per second multiplexed on 8 channels.

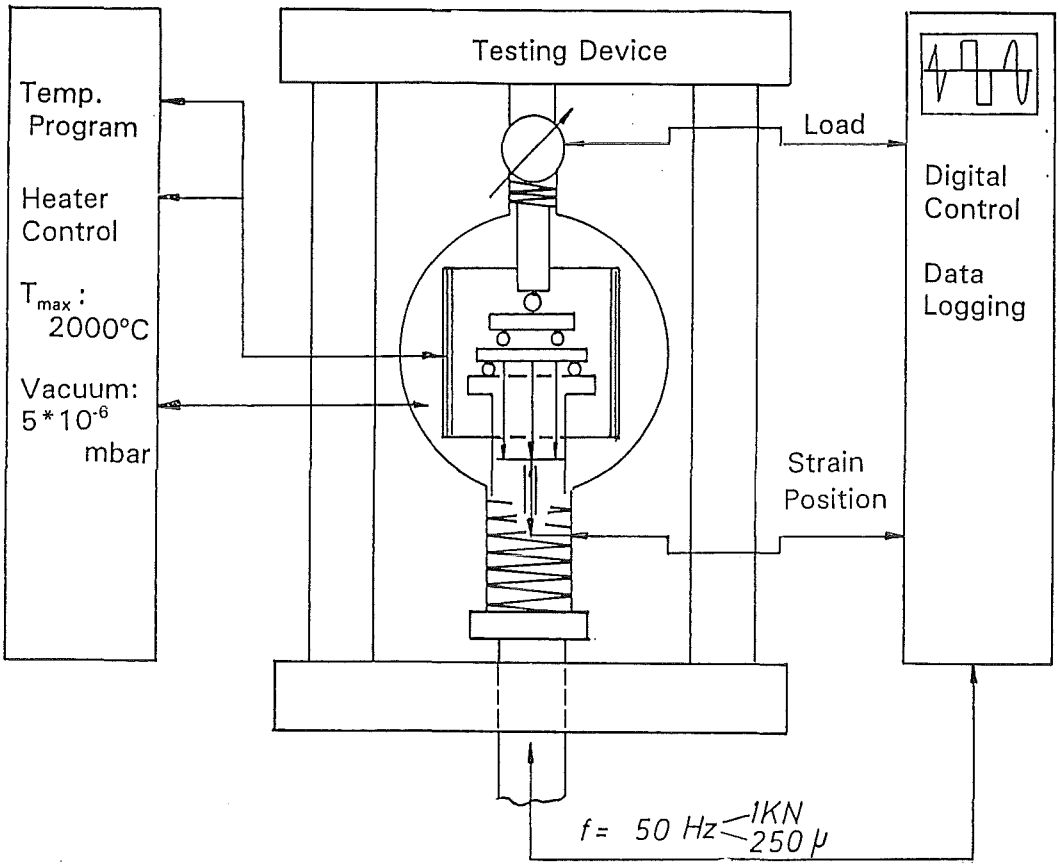

Figure 3. . Test facility for high-temperature, high-vacuum material testing.

3.2.2 Heater and vacuum device

The testing machine is equipped with a vacuum chamber and a tungsten radiation furnace. The vacuum device allows a total pressure lower than $5 \cdot 10^{-6}$mbar to be set at the high temperature. It is also possible to measure partial pressures of O_2, H_2O, *He*, *Ar*, H_2, *CO* and N_2 with a quadrupole mass spectrometer to determine gassing products of the carbon samples.
The heater consists of a tungsten meander heating wire and a tungsten multi-foil radiation heat shelter. The heating chamber is 100mm in diameter and reaches a maximum temperature of 2000°C.

3.2.3 Four-point-bending fixture

Inside the heating chamber a four-point-bending fixture is mounted, with an inner span of 20mm and an outer span of 40mm. The deflection of the specimen is measured by an LVDT (±1mm), which is positioned outside the furnace. The deflection of the sample is transmitted by three rods [4][5].

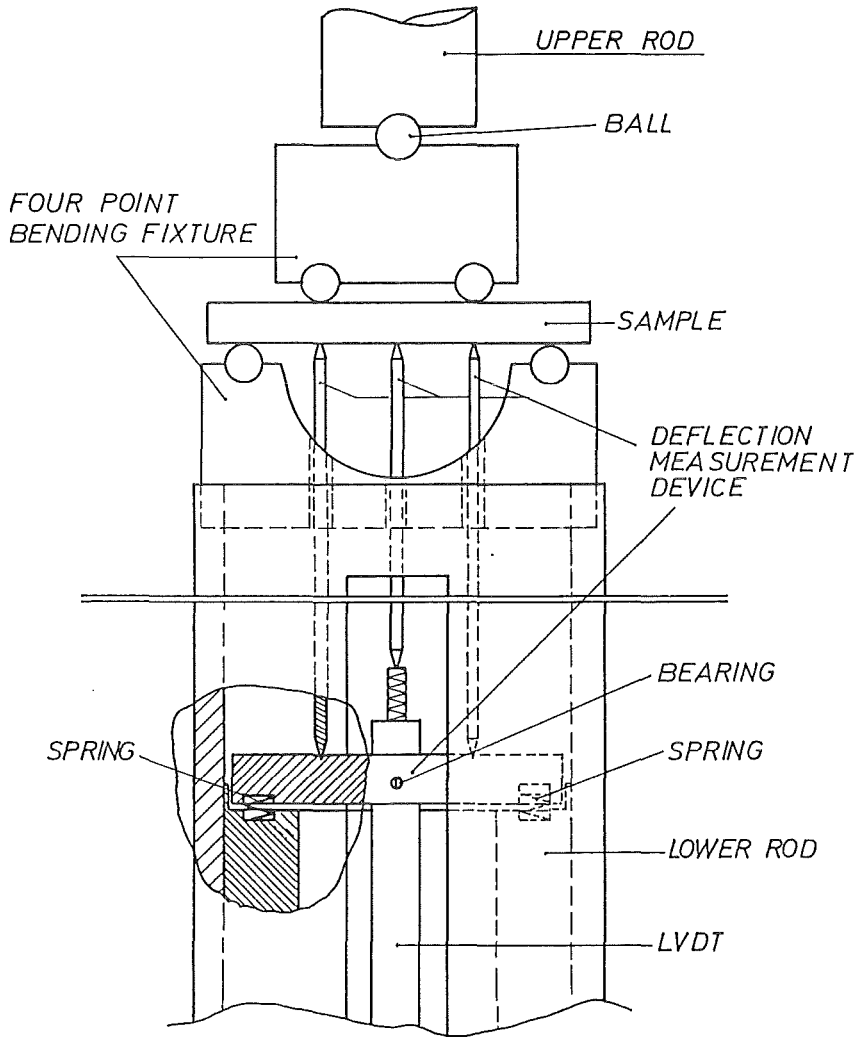

Figure 4. . Sketch of the four-point-bending fixture.

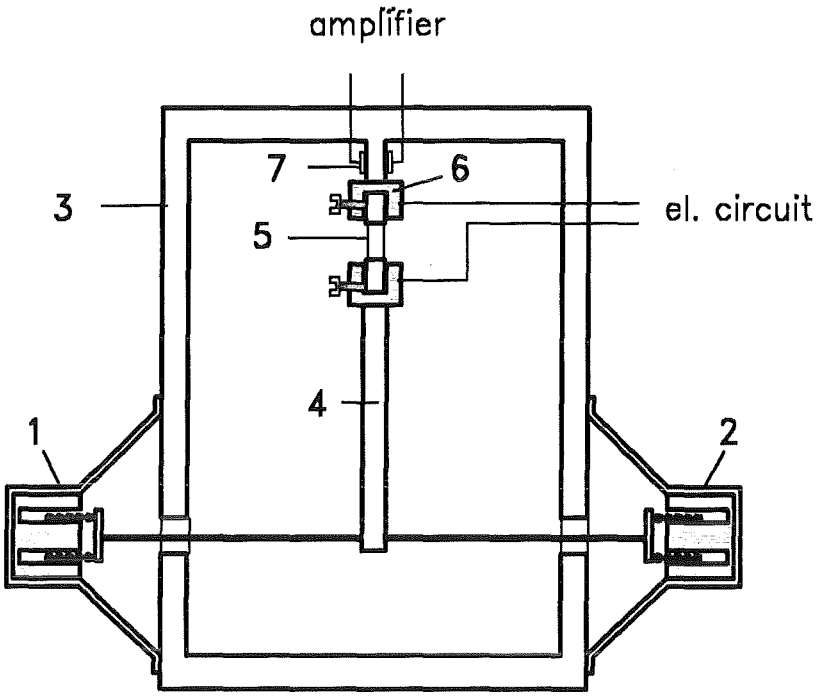

Figure 5. . Testing device for alternating bending tests [8].

3.3 Fatigue test arrangement

A simple testing device - developed at KfK [6][7] - operating with one loudspeaker was found to be best suited for resonance applications resulting in an excellent sinusoidal wave shape. To allow lower frequencies to be applied, the device had to be operated away from resonance. In this case, non-linearities of the load-displacement behaviour of ordinary loudspeakers have to be expected which may generate disturbing harmonics. Unfortunately, also the mechanical forces obtainable decrease.
Therefore, the apparatus was developed further [8]. The joint action of two loudspeakers results in a correction of non-linear distortions as well as in doubling of the load.
Figure 5 shows a simple testing device for cyclic bending tests with R=-1 [8]. The cyclic load is generated by the magnet system of the loudspeakers (1,2) - fixed at the frame (3) - and transferred to the specimen by a cantilever (4). The specimen (5) is clamped into the specimen holders (6) and the bending moment is measured by strain gauges (7) provided on the fixing bracket as well as directly on special specimens used for calibration.
The specimen itself (5) is fixed at its ends in brass tubes (8) by means of an epoxy resin (10) (see Fig.6). Due to the low Young's modulus of the epoxy resin compared with the Young's modulus of the ceramic specimen, the load can be applied without any notch effect. The second type of specimen fixing is recommended for materials with a relatively low Young's modulus. At the moment of failure, a silver strip (9) on the specimen

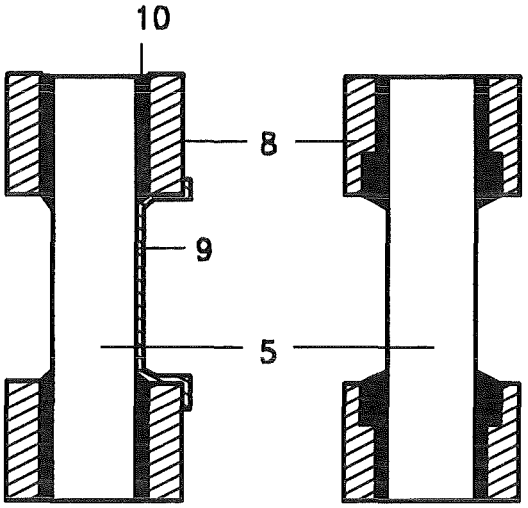

Figure 6. . Specimens used in fatigue tests.

is interrupted, the loudspeaker stops working and a time counter is stopped. The amplitude characteristic of the test arrangement is shown in fig.7 for a constant power supply. The squares indicate the bending moment measured with the strain gauges at location (7) of fig.5. The circles represent the signal for strain gauges applied at a calibration specimen (Al_2O_3). In fig.8 the ratio of the two signals is plotted vs. the frequency. It is obvious that no effect of frequency occurs for $f < 20$Hz. In case of higher frequencies the characteristic of the conversion factor has to be taken into consideration.

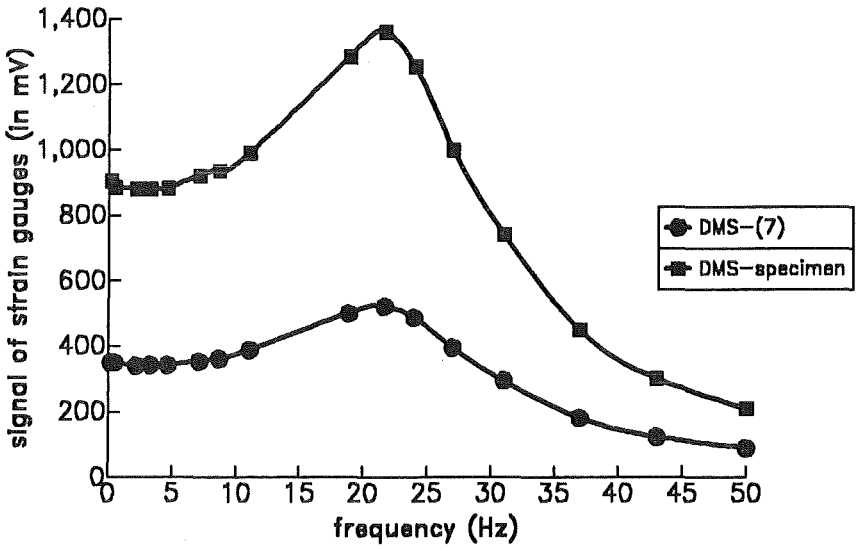

Figure 7. . **Fig.6a** Bending moment for constant power supply.

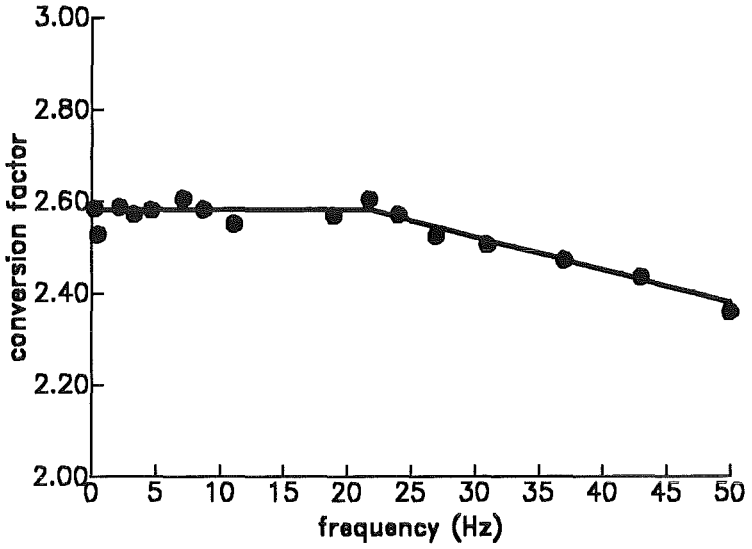

Figure 8. . Conversion factor between bending moment at the specimen and bending moment at the strain gauge (7).

3.4 Low-compliance bending test for R-curve determination

The measurement of R-curves can be performed in controlled fracture tests. In order to obtain stable crack extension a rigid test device must be used. A special testing arrangement has been developed at KfK [9] in which an extremely low compliance of the loading facility can be achieved (see fig.9). A further, more simplified testing device for controlled bending tests is shown in fig.10 where the load is generated by a screw. The effective load acting on the specimen is measured with the load-cell, and the displacement is recorded by an inductive displacement pick-up. In order to avoid additional compliances in the inner load circuit, it is recommended to use a quartz load-cell. If a testing machine is not available, the modification represented in fig.10 can be applied.

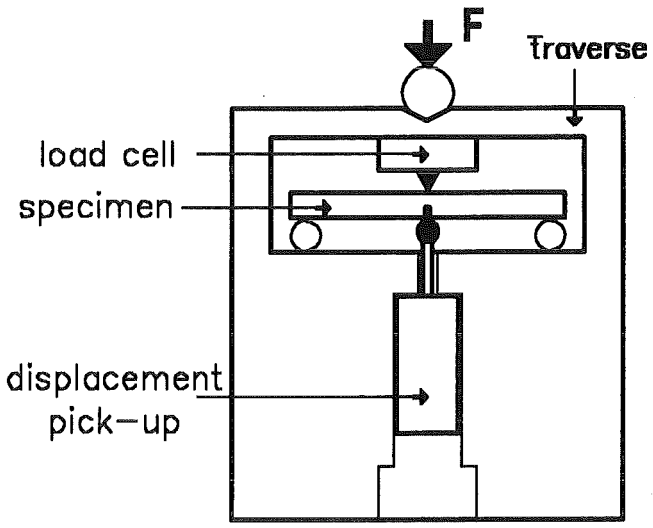

Figure 9. . Testing device for controlled fracture tests with loading by a strength testing machine.

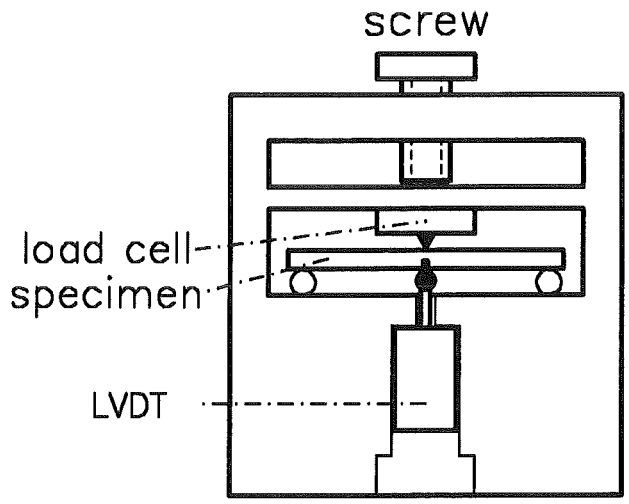

Figure 10. . Testing device for controlled fracture tests with simple loading by a screw.

4. Results

4.1 Bending strength at room temperature

In monolithic ceramics the strength of a specimen is related to the severest crack by the weakest link model resulting in a Weibull distribution of the strength. This model is, of course, not applicable to failure of CfC-materials, i.e. the maximum load is not the only consequence of the initial flaws. The failure behaviour is significantly influenced by the propagation phase of cracks, and crack growth resistance becomes part of the failure behaviour. Nevertheless, it is usual also for this type of material to represent the strength data as a Weibull-plot. In this type of diagram the failure probability F is plotted as a function of the strength σ_c, and the Weibull-parameters σ_0 and m are defined by the relation

$$F(\sigma_c) = 1 - \exp\left[-\left(\frac{\sigma_c}{\sigma_0} \right)^m \right] \tag{1}$$

Bending tests were performed in a cantilever test arrangement, as shown in fig.5, with a specimen as illustrated in fig.1. The test durations were about 2-3 seconds. The bending strength data (σ_c) for the different CfC materials at room temperature are shown in a Weibull representation: Material FMI 3333 in fig.11, N112(A) in fig.12, N112(B) in fig.14, N112(C) in fig.15. A comparison of all strength data - material N112(B) represented by the direction of highest strength - is given in fig.16. No significant differences between all materials tested were found.
From these data the Weibull-parameters m and σ_0 were determined by use of the Maximum-Likelihood procedure. In order to obtain an unbiased estimate m_{corr} for m, the bias factor $b(N)$ (N = number of tests) is introduced by Thoman et al. [10]. m_{corr} is given by

$$m_{corr} = m\, b(N) \tag{2}$$

where $b(N)$ can be approximated for $N > 5$ by [11]

$$b(N) \simeq \tanh^{1.87}\left(\frac{N - 3.855}{0.678} \right)^{0.21375} \tag{3}$$

All Weibull-parameters obtained have been summarised once more in Table 1.
In case of graphite only four specimens were available for the strength measurements and, consequently, a Weibull representation does not make any sense. The mean strength was $\overline{\sigma_c} = 50.0$MPa with a standard deviation of 5MPa.

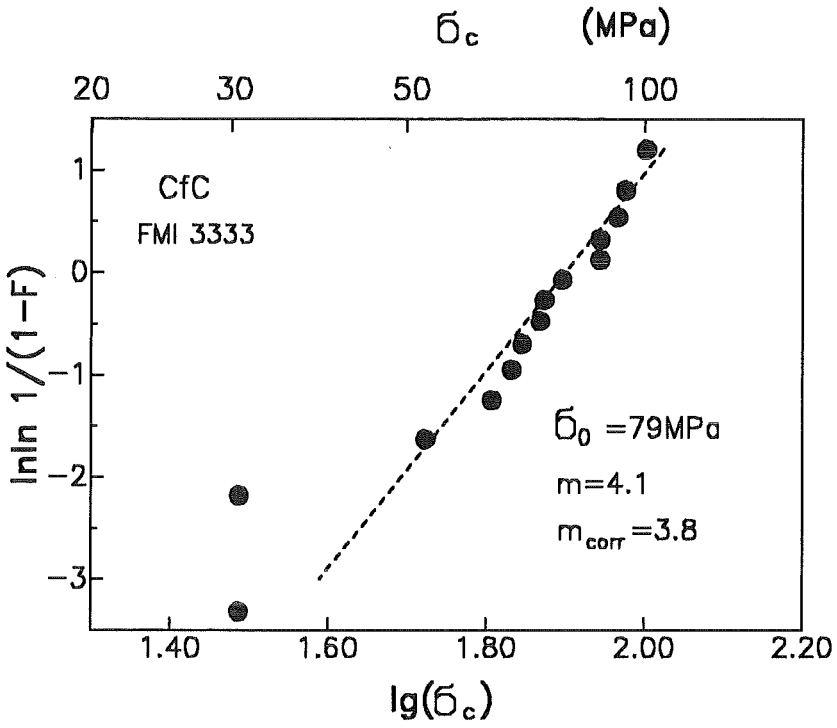

Figure 11. . Bending strength for FMI 3333 in a Weibull representation.

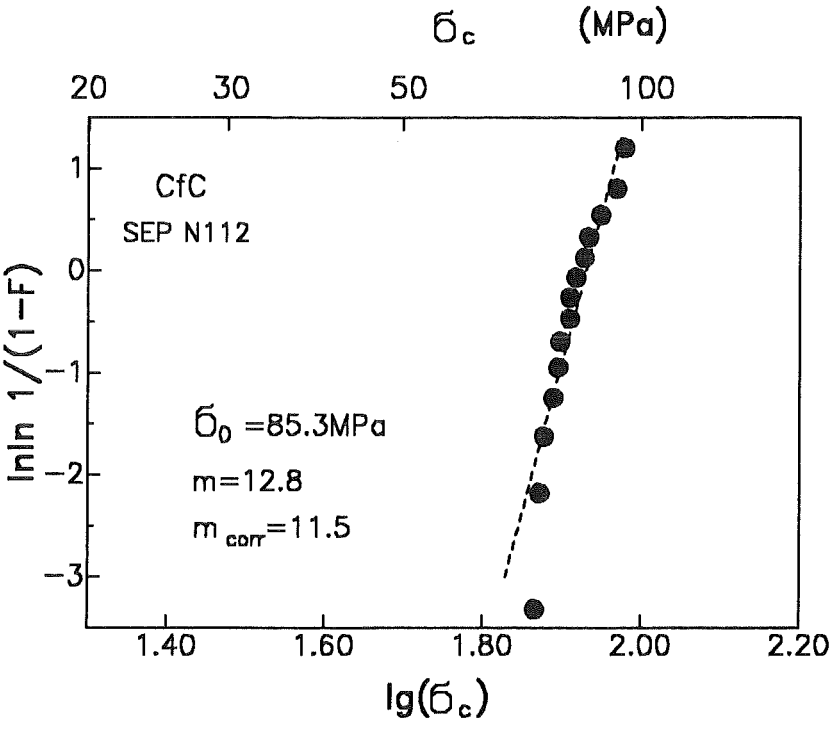

Figure 12. . Bending strength for N112(A) in a Weibull representation.

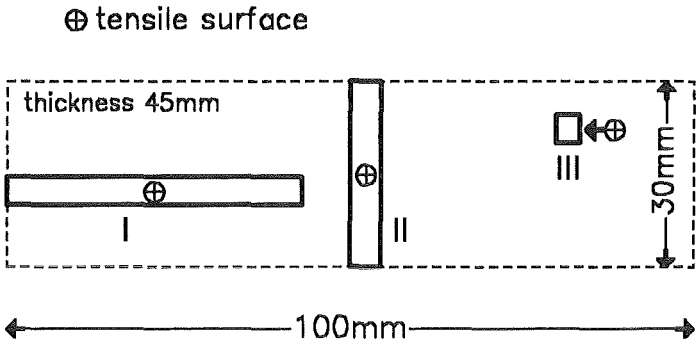

Figure 13. . Block cutting plane for material N112(B).

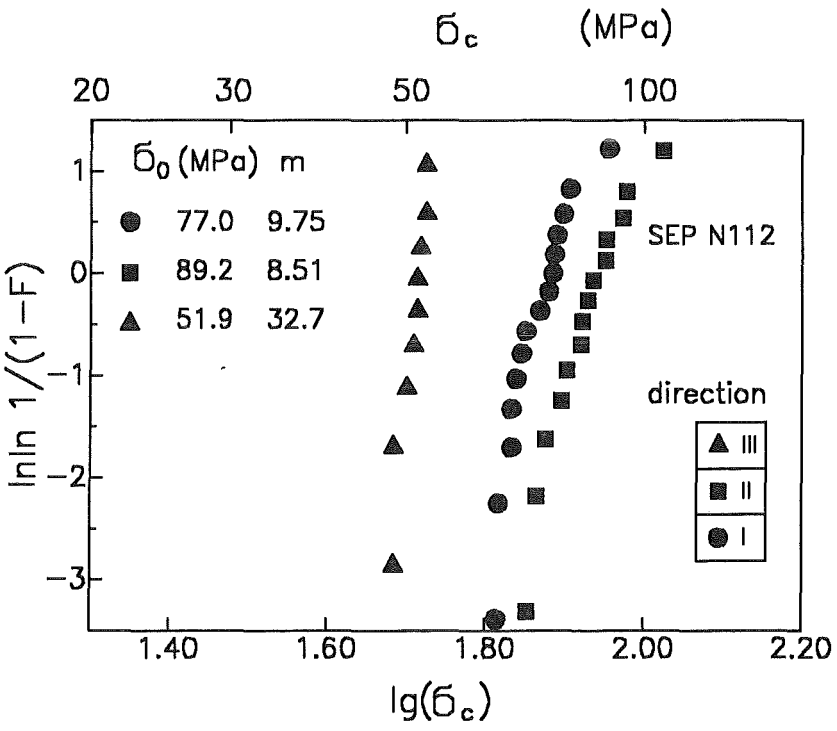

Figure 14. . Bending strength for N112(B) in a Weibull representation.

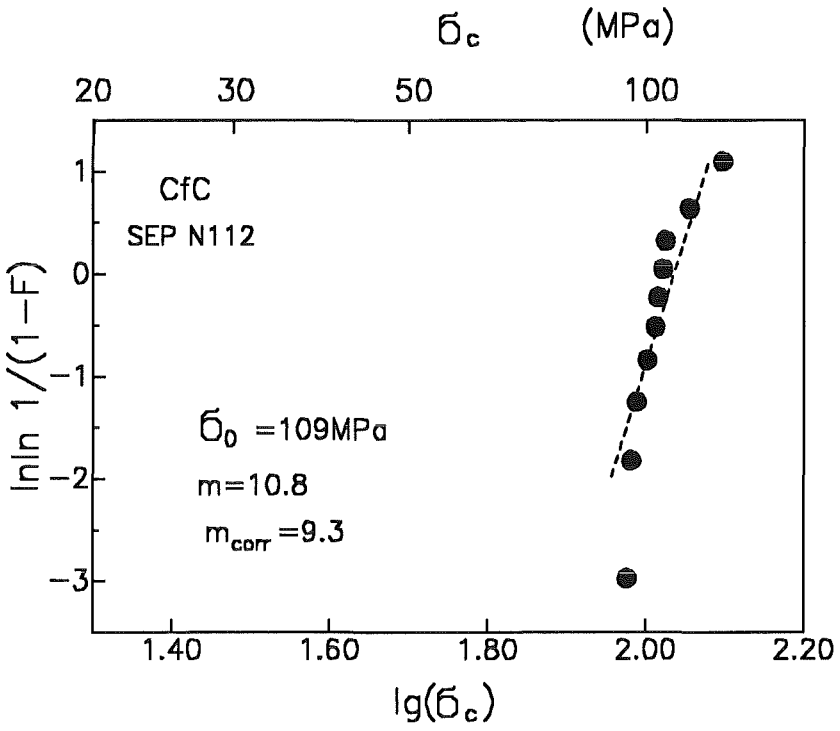

Figure 15. . Bending strength for N112(C) in a Weibull representation.

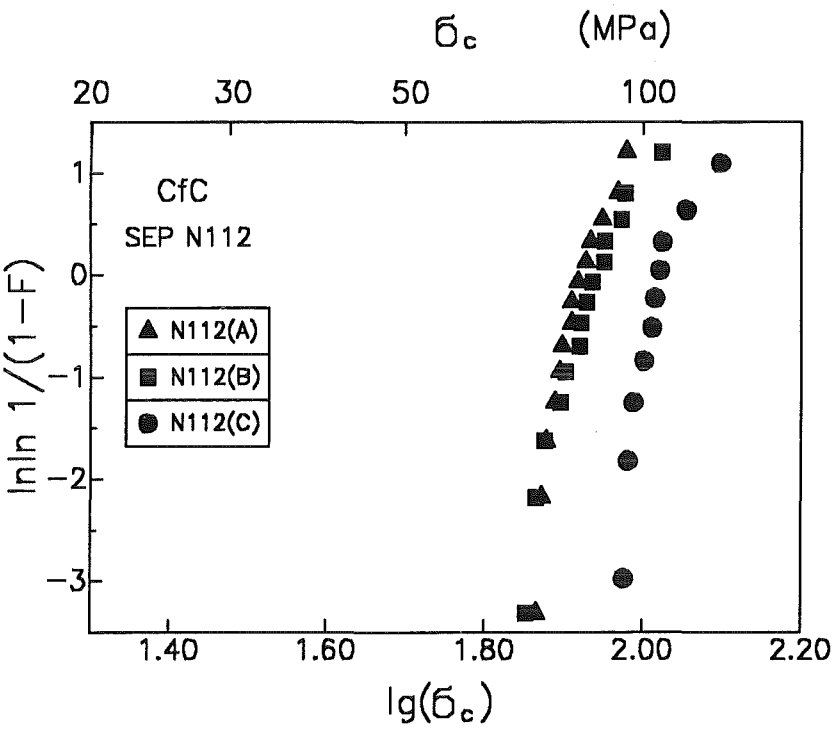

Figure 16. . Comparison of the different CfC-materials; in case of material N112(C) the direction of maximum strength is represented.

Material	Direc-tion	σ_0 (MPa)	m
FMI3333		79.0	3.8
N 112(A)		85.3	11.5
N 112(B)	I	77.0	9.75
N 112(B)	II	89.2	8.51
N 112(B)	III	51.9	32.7
N 112(C)		109.	9.3
N 112(D)		84.	16.
EK 98		50	

Table 1: Strengths of several CfC-materials.

Figures 17 and 18 show micrographs of fractured specimens.

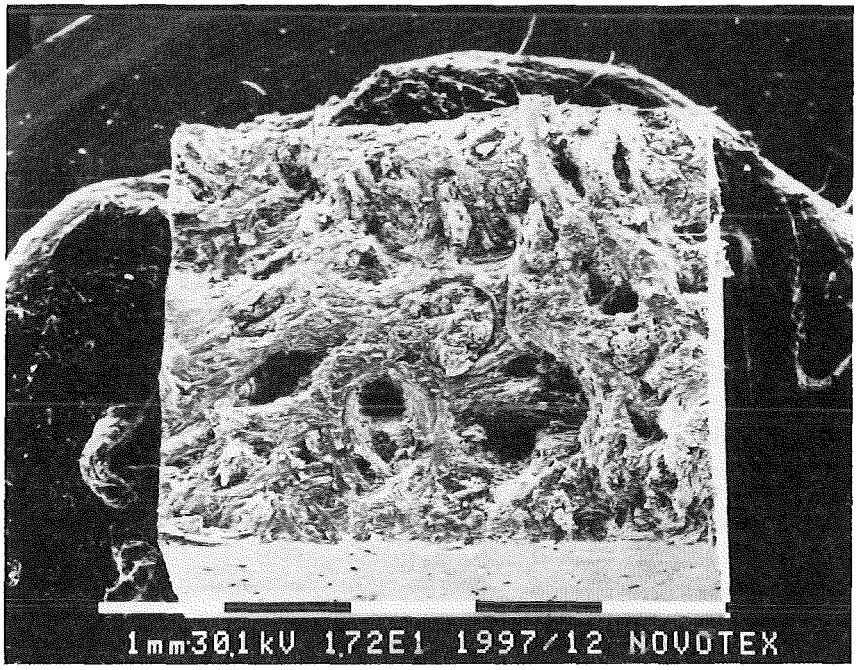

Figure 17. . Micrograph of a specimen (SEP N112) after a bending strength test.

The SEP-material shows a smooth fracture surface. For fibres which are parallel to the direction of loading a poor fibre bundle pullout can be seen. At greater magnification almost no significant single-filament pullout is visible but it is possible to discern the different layers of the CVI processed matrix. For the fibres perpendicular to the direction of loading empty fibre channels inside the matrix can be recognised. This is an indication of low interfacial strength, especially at the edges of the fibre bundle. All fibres

which do not coincide with the load direction may act as defects and initiate matrix cracks.

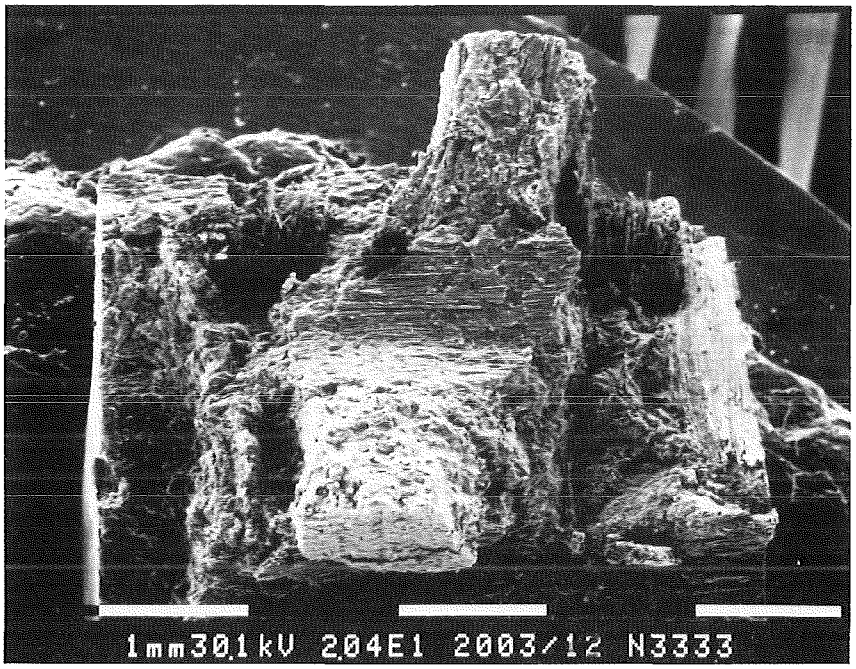

Figure 18. Micrograph of a specimen (FMI 3333) after a bending strength test.

The FMI 3333 specimen shows fibre bundles with large diameters. Parallel to the direction of loading, extensive fibre pullout is visible, while the only fibre bundle perpendicular to the load direction is scarcely delaminated. The cracks are propagating around these fibre bundles and are totally debonding them. The third fibre direction is $\pm 45°$ with respect to the axis. These fibres failed by shear.
The results for FMI 3333 show that the specimen size is too small for a correct evaluation of strength to be made.

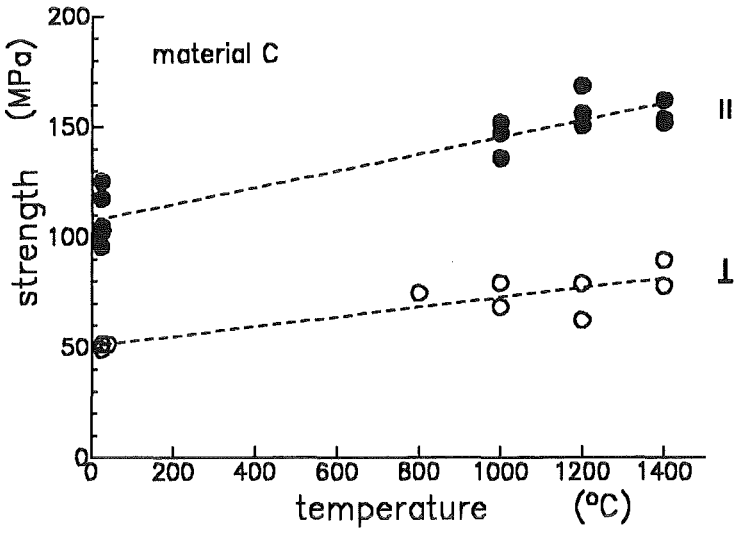

Figure 19. . High-temperature 4-point-bending strength; material N112(C).

4.2 High-temperature bending strength

Four-point bending tests were carried out with material N112(C) at elevated temperatures in the vacuum. The loading rate was chosen to be $\dot{\sigma} = 20\text{MPa/s}$. The results are represented in fig.19. An increase in strength with increasing temperature can be detected for both directions. The increase in strength with increasing temperature is about 4%/°C.

4.3 Cyclic fatigue

4.3.1 Cyclic fatigue of graphite

Figure 20 shows fatigue data obtained for graphite at $R = -1$ and $f = 50\text{Hz}$, where the R-ratio is defined by

$$R = \sigma_{min}/\sigma_{max} \tag{4}$$

Despite the large scatter of the data points, the following relation can be derived:

$$t_{f\,cycl} \propto (\sigma_{max})^{-90} \tag{5}$$

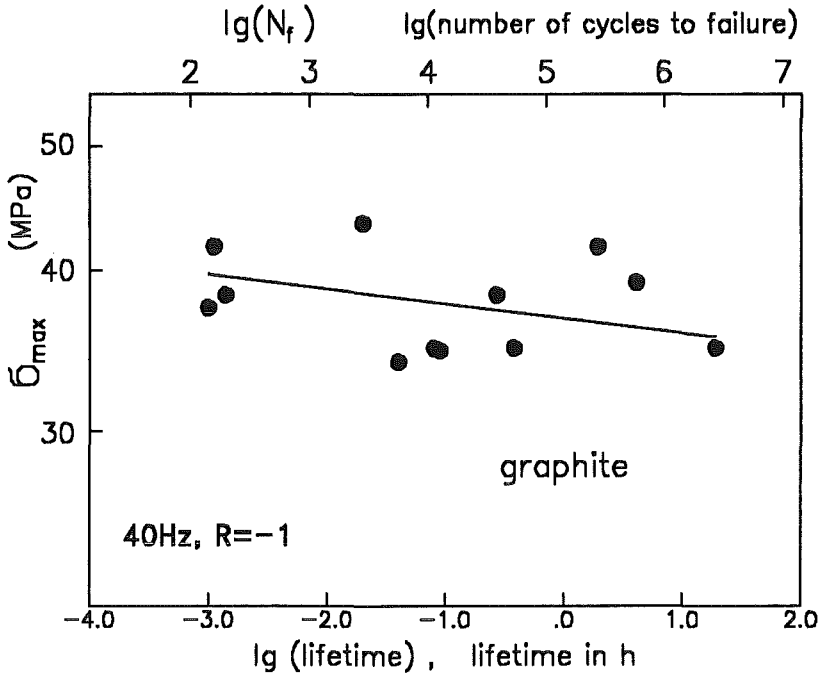

Figure 20. . Fatigue of fine graphite EK89.

4.3.2 Cyclic tests with SEP-N112

The fatigue of CfC-material N112(C) at R = -1 and f = 4Hz is shown in fig.21 as a Wöhler plot. A least-squares fit of these data gives

$$t_{f\,cycl} \propto (\sigma_{max})^{-75} \tag{6}$$

In real fusion reactor applications the loading conditions are between those in the two limit cases of load-controlled and displacement-controlled tests. This is also the case in cyclic tests with constant power supply. From this point of view this type of testing seems to simulate best the real conditions. In a previous test series cyclic loading tests were performed with the SEP-material. The frequency was chosen to be f = 1Hz and the electrical power supply was kept constant during one test. The maximum bending moment during the cycles was recorded with an XY-recorder. As can be seen from fig.22, the bending moment decreases with the number of cycles (i.e. with time). This behaviour may be explained by an increase in the specimen compliance due to an increase in internal damage.

4.4 R-curves

R-curves were determined for CfC-N112(B). Two crack resistance curves are shown in fig.23. The initial stress intensity factors K_{I0} for which initiation of crack growth occurs are relatively low ($K_{I0} \simeq 1 MPa\sqrt{m}$), but the increase with crack extension is extremely strong.

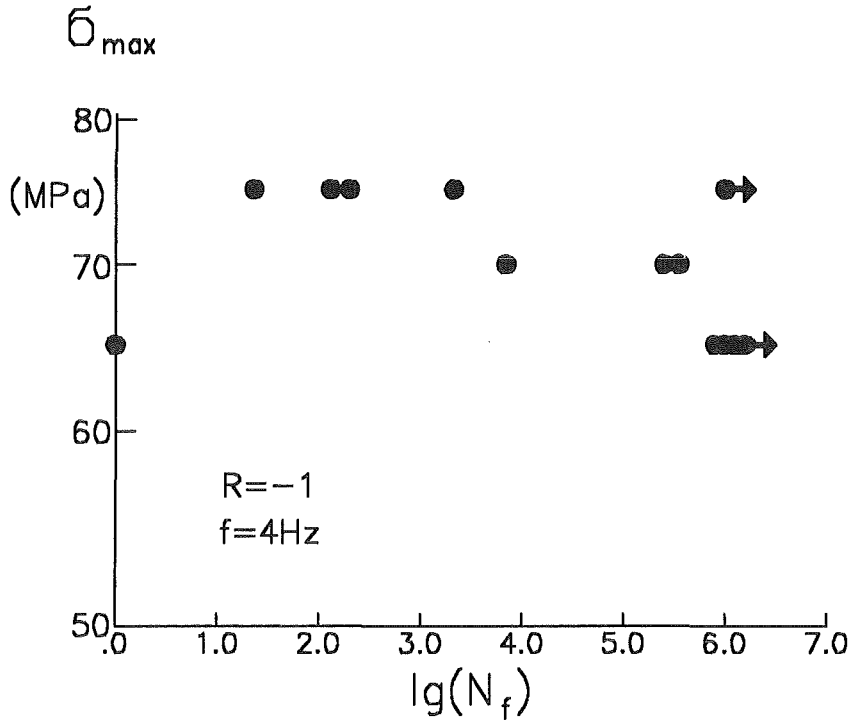

Figure 21. . Fatigue of CfC-material N112(C).

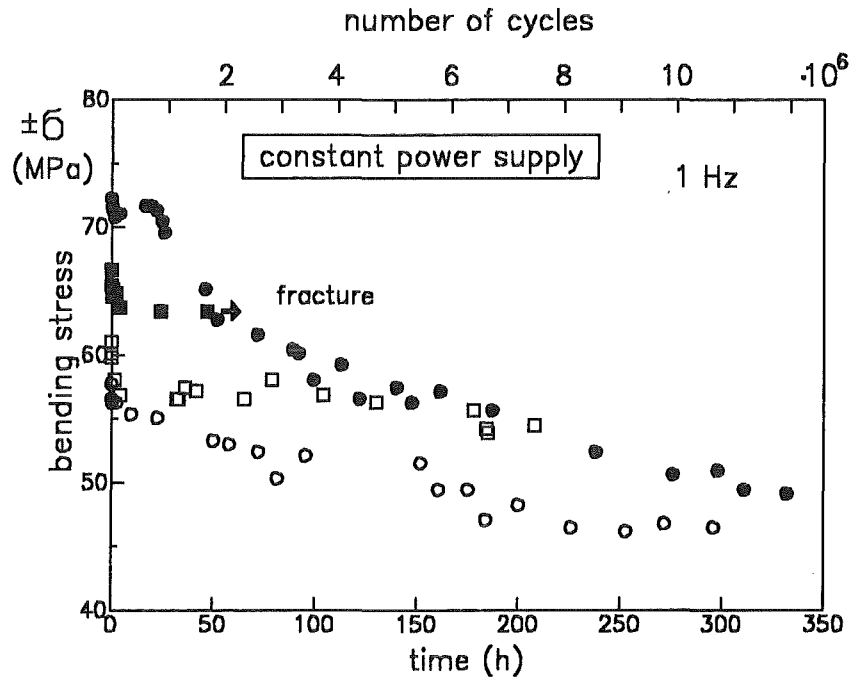

Figure 22. . Bending moment as a function of the number of cycles for a constant loudspeaker current, material N112(B).

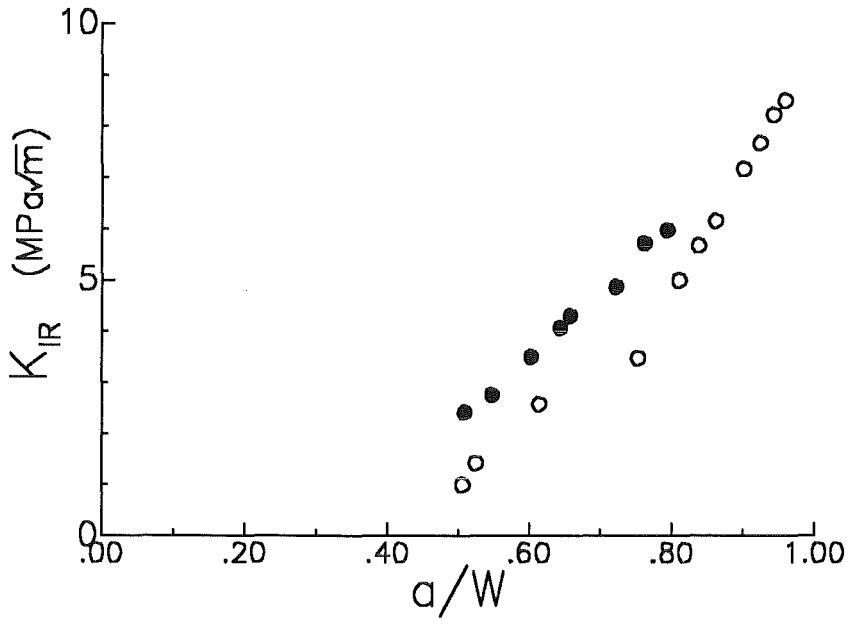

Figure 23. . Crack resistance curve for N 112 (B).

5. Microstructure

5.1 Microstructural investigation by optical microscopy

The specimens were prepared in the following steps:

- Cutting-off suitable pieces from an undamaged specimen.
- Embedding these specimens in ceramographic resin.,
- Grinding and polishing with diamond paste down to 1μm grain size.
- Use of an optional etching process to make parts of the microstructure stand out.

The SEP material is characterised by a multi-directional arrangement of the fibres. The diameter of the fibre bundles is almost 200μm, the diameter of single filaments about 5-8μm, as shown in fig.24.
A magnification of 1000x (see fig.25) reveals the various layers of the matrix. The microstructure is quasi-homogeneous. In contrast to this, the FMI 3333 material shows (cf. fig.26 and fig.27) very large fibrebundles (diameter up to 1000 μm) and fibres with a wide variation of the diameters from 5μm to 10μm. Inside the fibre bundles the fibres are very densely packed, in a kind of hexagonal structure, where every fibre is in contact with the neighbouring fibre. It is generally noticed that there are large cracks in the matrix between fibre bundles of different orientations.

5.2 Microstructural investigation with the scanning electron microscope

The specimens were prepared in the following steps:

- Cutting off suitable pieces from a fractured specimen.
- Cleaning the specimens with a mixture of ethanol and toluene.
- Fixing the specimens on an SEM slide.

Corresponding to the deviating mechanical properties, the fracture surfaces of SEP N112 and FMI 3333, respectively, also show differences. The SEP material shows a smooth fracture surface (fig.28). For fibres which are parallel to the load direction a poor fibre-bundle pullout can be observed [12]. At higher magnification (fig.29) almost no signif-

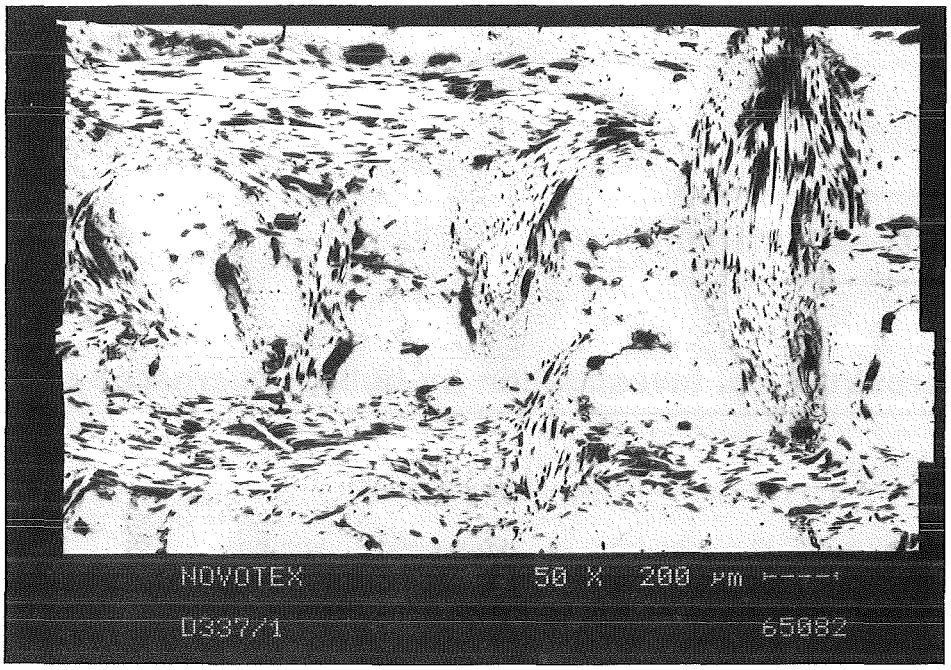

Figure 24. . Optical micrograph of N112(A); magnification x50.

icant single filament pullout can be observed, but it is possible to discern the various layers of the CVI-processed matrix.

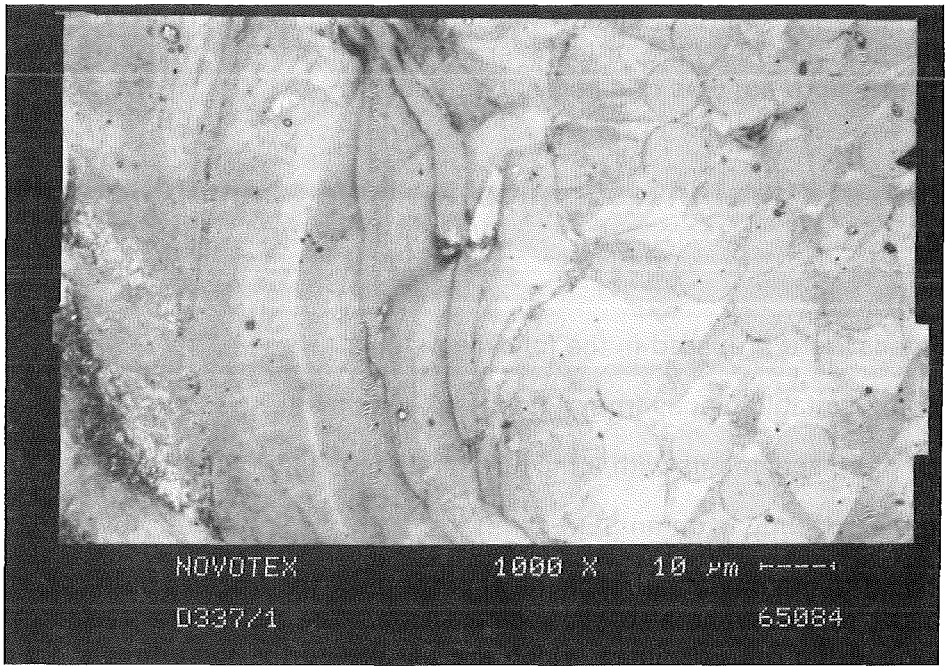

Figure 25. . Optical micrograph of N112(A); magnification x1000.

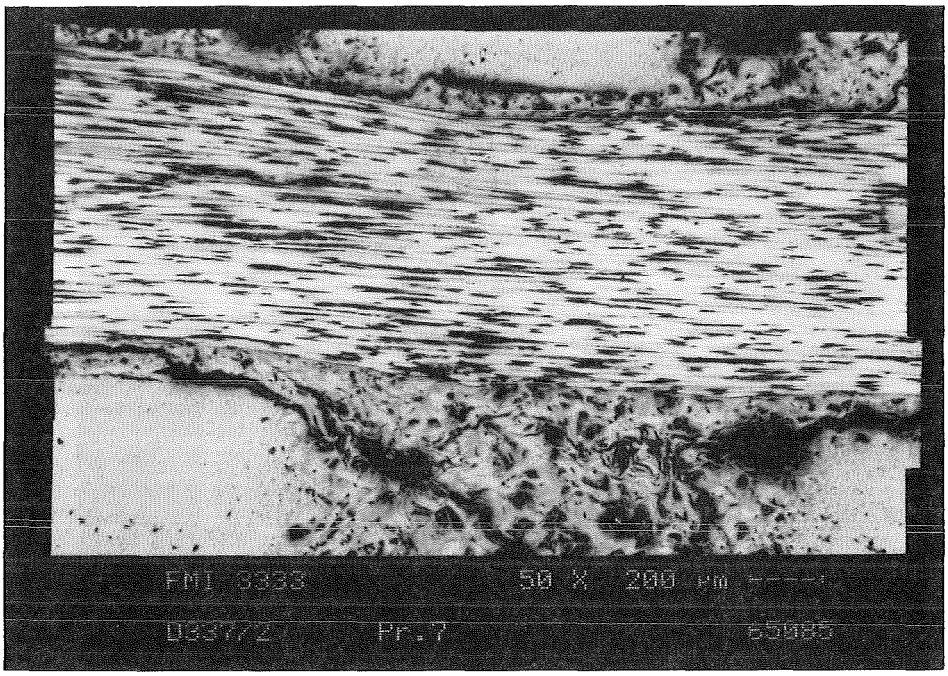

Figure 26. . Optical micrograph of FMI 3333; magnification x50.

For the fibres perpendicular to the load direction empty fibre channels are visible inside the matrix. This is an indication of low interfacial strength, especially at the edges of the fibre bundle. All fibres which do not run in the direction of loading may act as defects

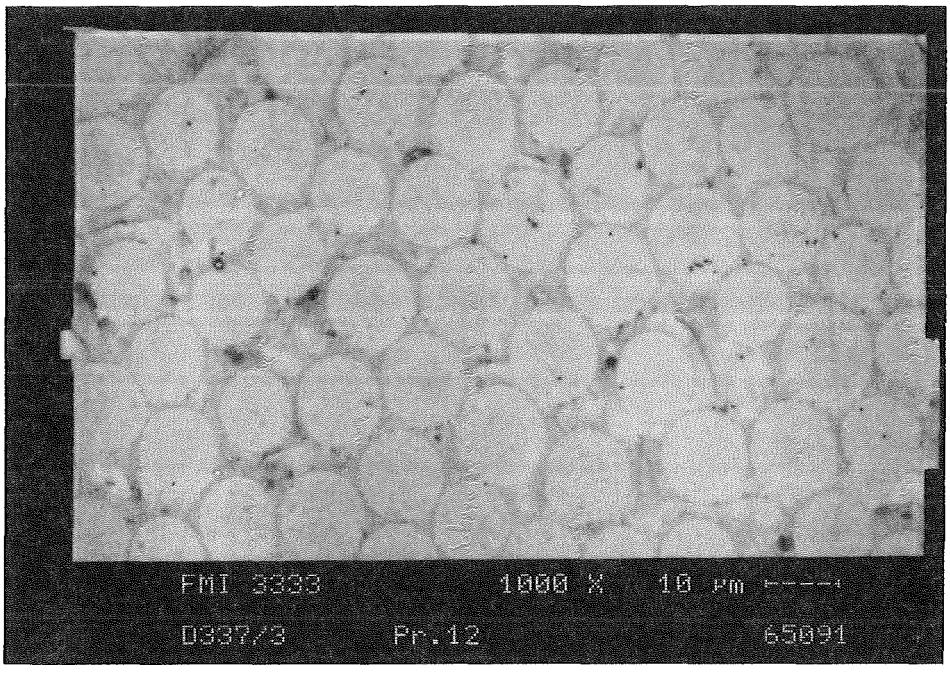

Figure 27. . Optical micrograph of FMI 3333; magnification x1000.

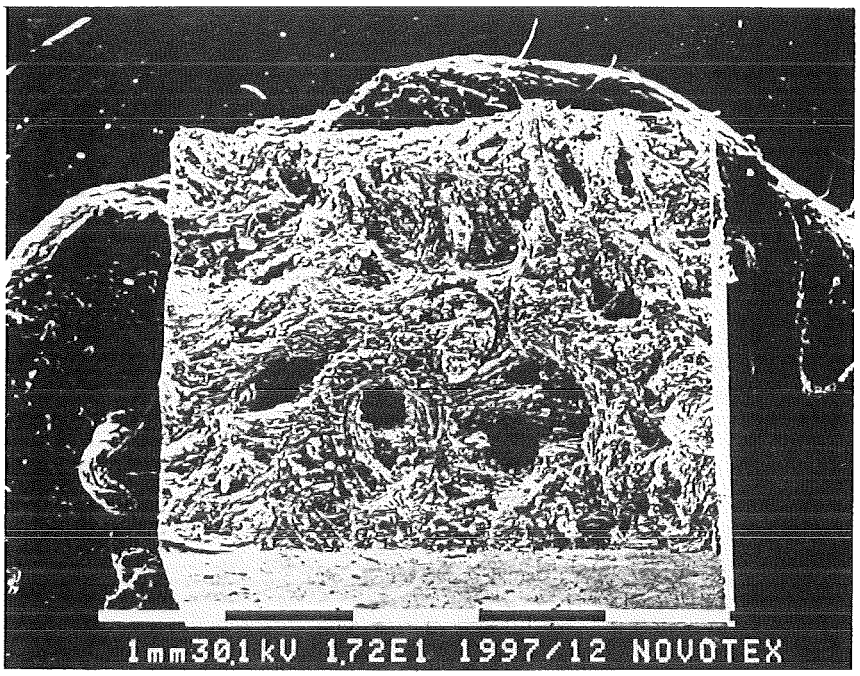

Figure 28. . Fracture surface of material N112(A) at a magnification x20.

and initiate matrix cracks. Many intermediate stages exist between the differences in behaviour of fibres parallel or perpendicular to the load direction.

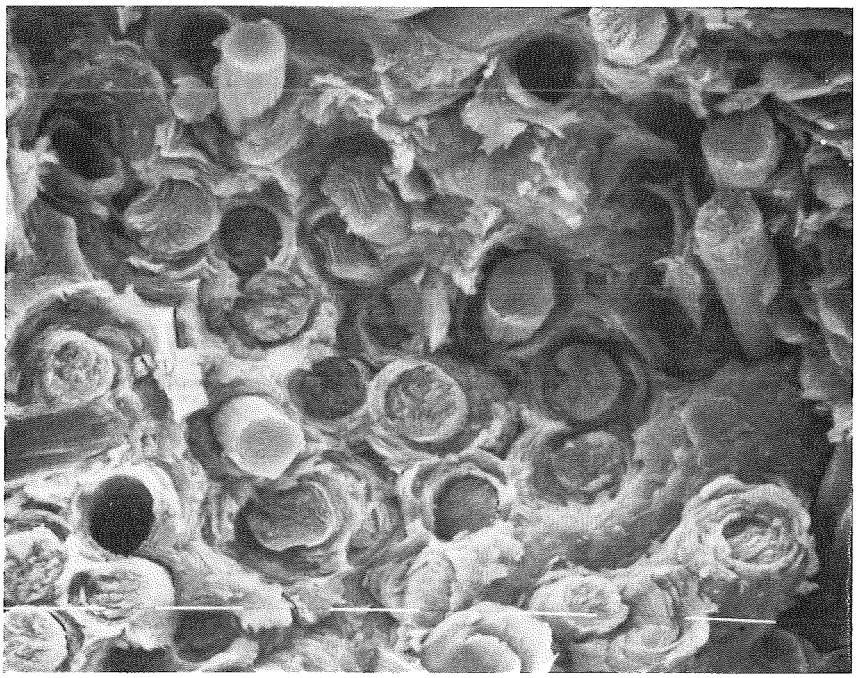

Figure 29. . Fracture surface of material N112(A) at a magnification x1250.

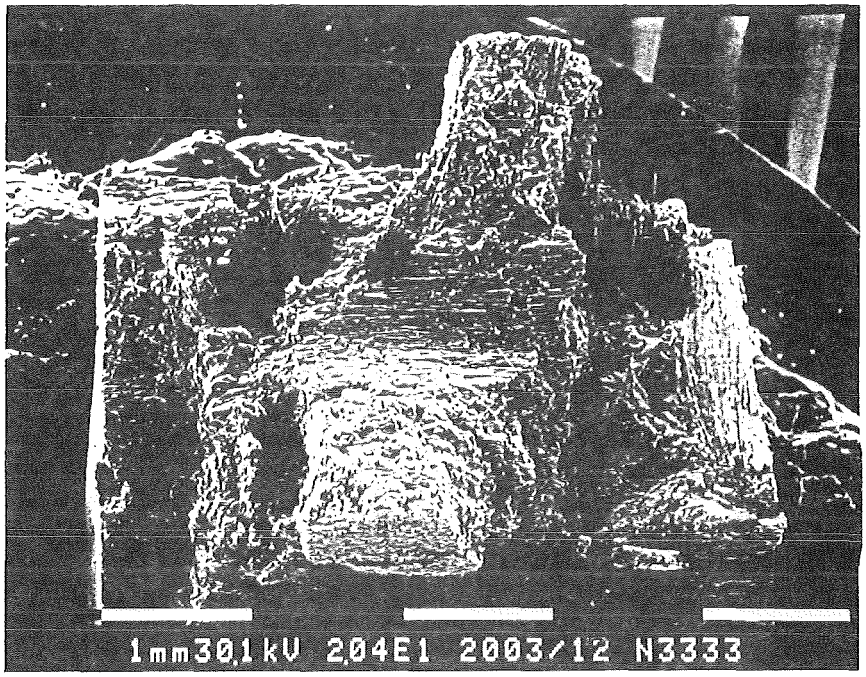

Figure 30. . Fracture surface of material FMI 3333 at a magnification x20.

The FMI 3333 specimens show fibre bundles of very large diameters. Parallel to the load direction, extensive fibre pullout is visible, while the only fibre bundle perpendicular to the load direction is scarcely delaminated (fig.30). It appears that the cracks are

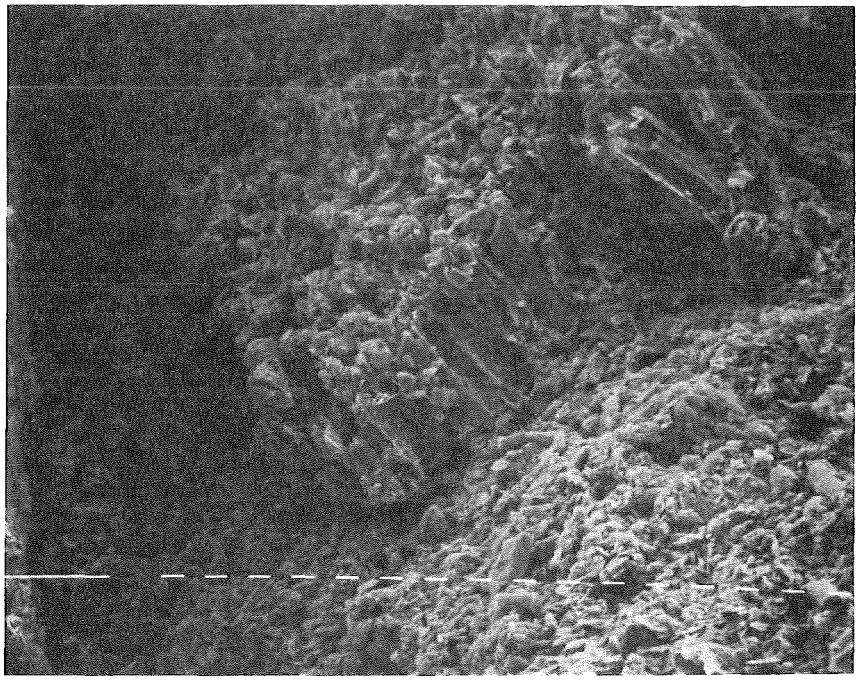

Figure 31. . Fracture surface of material FMI 3333 at a magnification x320.

propagating around these fibre bundles and debonding them totally, if they are not already debonded. The third fibre direction is +45° with respect to the axis. These fibres failed through shear (see fig.31). All these results show that the specimen size for the FMI 3333 seems to be too small in this bending test for a correct evaluation of strength to be made and that they have to be increased before further experiments with this material can be performed.

6. References

[1] T.v. Karman, Über die Grundlagen der Balkentheorie, Abhandlungen aus dem Aerodynamischen Inst. der TH Aachen **7**(1927).

[2] F. Seewald, Die Spannungen und Formänderungen von Balken mit rechteckigem Querschnitt, Abhandlungen aus dem Aerodynamischen Inst. der TH Aachen **7**(1927).

[3] D. Munz, T. Fett, Mechanisches Verhalten keramischer Werkstoffe, Reihe: Werkstoff-Forschung und -Technik 8, Springer-Verlag Berlin 1989.

[4] T. Fett, K. Keller, G. Martin, O. Rosenfelder, J. Test. and Eval. 19(1991),334-337.

[5] T. Fett, K. Keller, G. Martin, O. Rosenfelder, Patentschrift DE 3629131 C2 (1988).

[6] T. Fett, G. Martin, D. Munz, G. Thun, Determination of da/dN-ΔK_I-curves for small cracks in alumina in alternating bending tests, to be published in J. Mater. Sci..

[7] T. Fett, G. Thun, German Design Patent G 8911720.4.

[8] T. Fett, G. Thun, German Design Patent G 9107645.5.

[9] T. Fett, G. Thun, German Design Patent G 9207089.2.

[10] D.R. Thoman, L.J. Bain, C.E. Antle, Inferences on the parameters of the Weibull-distribution, Technometrics **11**(1969)445-460.

[11] T. Fett, D. Munz, G. Thun, Influence of frequency on cyclic fatigue of coarse grained Al_2O_3, to be published in J. Mater. Sci. Letters.

[12] F. Ansorge, T. Fett, E. Hoffmann, unveröffentlichter Bericht, Kernforschungszentrum Karlsruhe, Nov. 1991.

[13] H. Zimmermann, Festigkeit und elastische Eigenschaften einiger Graphit-, CfC- und SiC/SiC-Materialien, KfK-Report 5371, 1994.

[14] T. Fett, H. Zimmermann, Mechanical behaviour of CfC-Sepcarb N112 at room-temperature, SOFT 18, Karlsruhe, August 22-26 1994.

[15] S. Spinner, W.E. Tefft, Amer. Soc. Test. Mat. **61**,1221(1961).

7. Appendix

7.1 Elastic moduli

Knowledge of elastic moduli is necessary to compute thermal stresses. Zimmermann [13] has investigated several materials. The elastic properties, Young's modulus E, and shear modulus G were determined by measuring the oscillation periods of bending and torsional vibrations with a Grindo Sonic device. The test object is excited by means of a light external impulse in such a way that the desired vibration mode is attained. The vibrations are picked up by a microphone or by a piezoelectric transducer, and a measuring circuit determines the resonant frequency which is used to calculate the elastic moduli according to Spinner and Tefft [15]. The tests were carried out in different regions of two plates and the results are entered in Table 2 ([13] [14]). Figure 32 shows the locations of the block wherefrom the specimens had been taken. Additionally, strength measurements were carried out for all these locations and the results are entered in Table 2.

Plate	Region	Bending strength σ_0(MPa), m	Shear strength (MPa)	E (GPa)	G (GPa)
1	I	83.7; 16	10.3±0.7	27.2±1.8	6.7±0.2
	II	83.1; 13.4	9.8±0.6	24.9±3.3	7.5±0.5
	III	88.5; 15.6		26.6±3.4	
	IV	86.2; 9.1	10.7±1.1	27.3±1.3	5.4
	V	81.0; 7.6	6.9±0.7	24.6±2.2	5.0
	VI	69.4; 6.9	10.0±1.1	14.1±4.7	5.1
	VII	60.9; 8.6	6.6±0.9	16.9±0.2	6.3
2	I	99.2; 14.1	11.3±1.3	32.1±3.5	

Table 2: Influence of location on strength and elastic moduli.

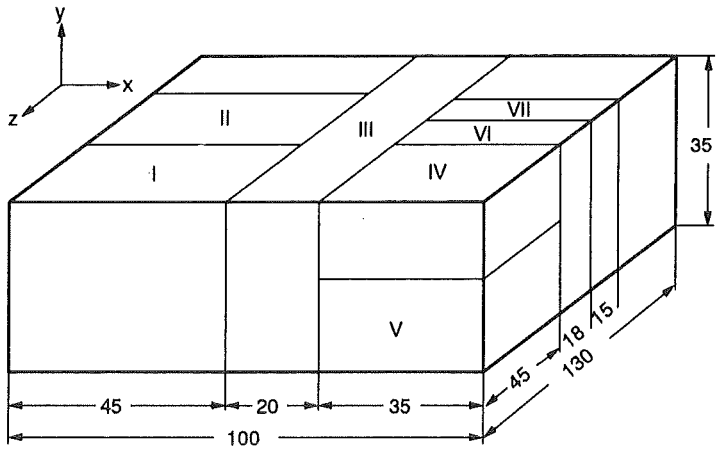

Figure 32. . Location of test specimens